The Effects of Specimen Size and Testing Conditions on Fracture Toughness Evaluation of Polypropylene Homopolymer

EDGARDO SANTARELLI

Departamento de Mecánica Aplicda
Universidad Nacional del Comahue
Buenos Aires 1400
8300 - Neuquén, Argentina

and

PATRICIA FRONTINI*

Instituto en Ciencia y Tecnología de Materiales
CONICET-Universidad Nacional de Mar del Plata
7600 - Mar del Plata, Argentina

The results of an experimental test program performed to investigate the influence of specimen dimensions and testing rate conditions on room temperature fracture toughness of PP homopolymer are presented. The material displayed nonlinear load-displacement behavior and exhibited small amounts of slow crack growth (ductile tearing) prior to cleavage instability, which invalidates the direct application of the current standards for the determination of K_{IC} in polymers. Data points were considerably scattered consistently with typical ductile-brittle transition patterns. The resulting load-displacement diagrams were analyzed in terms of K_Q, K_{MAX}, and the ratio P_{MAX}/P_Q. The fracture toughness at instability, J_C, was also computed and plotted against the amount of stable crack growth in order to construct J-R curves as a function of size and strain rate. From these curves an alternative critical fracture parameter, K_{JIC}, was calculated. Weibull statistics were used as a tentative approach for treating the scatter of fracture toughness of polypropylene homopolymer in large samples, which exhibited restricted ductile tearing. The significance of each of these methods and the validity and size independence of the corresponding parameters are discussed.

INTRODUCTION

Fracture properties of Polypropylene polymers and their rubber blends have been extensively studied (1–3). The lack of toughness and the brittleness exhibited by PP homopolymer at room temperature were explained in terms of the nearness of its Tg to room temperature. However, the direct application of LEFM (4–6) in this kind of material is not so simple because of the nonlinear characteristic of load-displacement plots and the variations in constraint, which affect the fracture toughness values determination. Several authors (1–3) attributed size dependency to plane stress skin effects and used a single additive model to take into account the plane stress and plane strain contributions to toughness. Plane strain lower-bound toughness was determined at temperatures well below room temperature (at −60°C) (2) by extrapolating apparent toughness to infinite-thickness sample.

Fernando and Williams (2) found that the homopolymer exhibited small amounts of slow crack growth (ductile tearing) above 0°C and became completely ductile above 30°C. To avoid taking into account the effect of ductile tearing (stable crack growth), they smartly studied fracture far away from ductile-brittle transition temperature. Analogous ductile-to-brittle transition regime behavior and / or transition from stable to unstable crack propagation regime was reported for similar materials under

*Corresponding author.

diverse testing conditions, in more recent papers (7–12).

To obtain meaningful PP homopolymer fracture toughness data at room temperature (ductile-brittle transition regime) is extremely difficult. Values are often highly scattered and show a strong sensitivity to geometry dimensions and strain rate. In addition, some tests exhibit excessive nonlinearity of load-line displacement plots and the presence of stable crack extension prior instability, which compromise the validity of classic LEFM methodologies (4–6). This paper presents the results of a wide experimental study on the influence of strain rate and geometry dimensions, which affect in-plane and out-plane-constraint effects. We aim at giving additional insight into the determination of significant fracture toughness values of PP homopolymer, which still appears controversial.

EXPERIMENTAL

Materials and Processing Conditions

Studies were performed on a commercial extrusion-grade isotactic polypropylene (PP), produced by Petroquímica Cuyo with the trade name of Cuyolen PP 1102 KX, MFI: 3.4 g/10 min. Pellets were compression molded into thick plaques at 200°C and 4.3 MPa and then rapidly cooled with running water. The plaques were then annealed in an oven for 3 h at 90°C to release thermal stresses generated during molding. Crystallinty measured by DSC (13) was 60%.

Specimen Preparation and Test Conditions

Fracture characterization was carried out on three-point bend specimens (SENB), cut from the compression-molded plates over a broad range of dimensions (Thickness, B, was varied between 3.5 and 21 mm; and the depth, W, was varied between 7 and 42 mm). Span, S, to depth ratio and crack to depth ratio were always kept equal to 4 and 0.5, respectively. Proportional (B/W = 0.5) and non-proportional specimens (B/W ≈ 0.37 and 0.23) were also assayed. Samples were machined to reach final dimensions and improve edge surface finishing. Sharp notches were introduced by scalpel-sliding a razor blade having an on-edge tip radius of 0.13 mm. In some specimens, sidegrooves of equal depth were machined into each face to give a total reduction in thickness of 0.2B. To be sure that data scatter did not arise from eventual differences in processing conditions among different plaques, thin specimens were obtained from the arms of thicker specimens after being tested.

Tangent Elastic modulus, E, and yield stress, σ_y (taken at maximum of load-displacement trace), were determined in tension on dumb-bell specimens machined from strips transversely cut from the 21-mm-thick plaques as a function of strain rate as shown in *Fig. 1*.

Mechanical tests were carried out at room temperature and varying crosshead rate, v, between 3 and 10 mm/min in an Instron 4467. Fracture-tested specimens were loaded monotonically to failure, and load and displacement were monitored. In some experiments the initial loading velocity was controlled in order to give constant bending nominal strain rate calculated following *Eq 1*, (14).

$$\dot{\varepsilon} = \frac{6vW}{S^2} \tag{1}$$

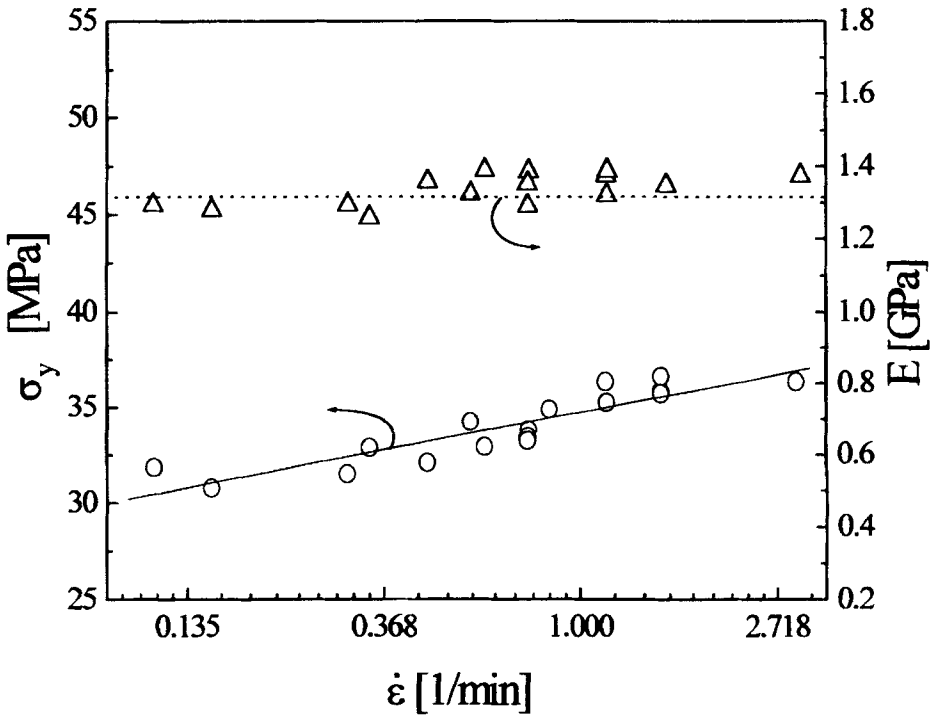

Fig. 1. Yield stress and elastic modulus as a function of strain rate.

FRACTURE MECHANICS CALCULATIONS

From load-line displacement plots and crack length, the stress intensity factor, K, was computed from *Eq 2*, where f(a/W) is a dimensionless function of a/W (4–6),

$$K = \frac{P}{BM^{1/2}} f(a/W), \tag{2}$$

according to ASTM D5045 standard at maximum load (K_{MAX}) and at the special load value called P_Q load (K_Q). This latter procedure implies the determination of P_Q at the intersection between a straight line having compliance 5% greater than that of initial compliance and the load-displacement trace (*Fig. 2*).

For side-grooved specimens, effective instead of nominal thickness (15) was used:

$$Beff = \sqrt{BB_{net}}, \tag{3}$$

where the net thickness, B_{net}, is the distance between the roots of the side-grooves.

The conditional K_Q value computed with *Eq 2* is a valid K_{IC} (Critical Stress Intensity Factor in Mode I) result only if all validity requirements in the standard (4–6) are met, including:

$$0.45 \le a / W \le 0.55, \tag{4}$$

$$B,a,(W - a) \ge 2.5\left(\frac{K_Q}{\sigma_y}\right)^2, \tag{5}$$

$$\frac{P_{MAX}}{P_Q} \le 1.10. \tag{6}$$

The above-mentioned LEFM validity criteria were empirically derived to ensure the resulting K_{IC} to be size independent. This requires that the test be performed in plane strain under nominally linear elastic conditions.

Besides the calculation of K_Q, the value of the J-Integral at the instability point, J_C (*Eq 7*), (16, 17), and the amount of ductile tearing, Δa_c (measured directly from fracture surfaces) were recorded as well.

$$J_c = \frac{2\,U_c}{B(W - a)}. \tag{7}$$

The results are presented as a multispecimen J-R curve based on ductile crack growth value at cleavage initiation (18). A critical initiation value J_{IC} was determined at the intersection of the theoretical blunting line (*Eq 8*) and the J-R curve.

$$J = 2\sigma_y \Delta a. \tag{8}$$

A critical stress intensity factor was derived from J_{IC} using the following expression:

$$K_{J_{IC}} = \sqrt{\frac{EJ_{IC}}{(1 - \upsilon^2)}} \tag{9}$$

RESULTS AND DISCUSSION

Phenomenology

Loadline-displacement curves were smooth and deviated from linearity (*Fig. 2*). At a certain deflection level, sudden instability occurred and the specimen broke in two halves, which literally flew away aided by the energy provided by the elastic strain energy stored in the sample.

As explained in the specific literature (19), nonlinearity may be caused by plasticity, subcritical crack growth, or both phenomena. Fracture surfaces analysis (*Fig. 3a* and *3b*) revealed the presence of subcritical crack growth. The stable crack growth, which always preceded brittle fracture, is clearly demarcated in the photo and can be distinguished from the white halo corresponding to the damaged zone generated before crack propagation. The amount of the ductile

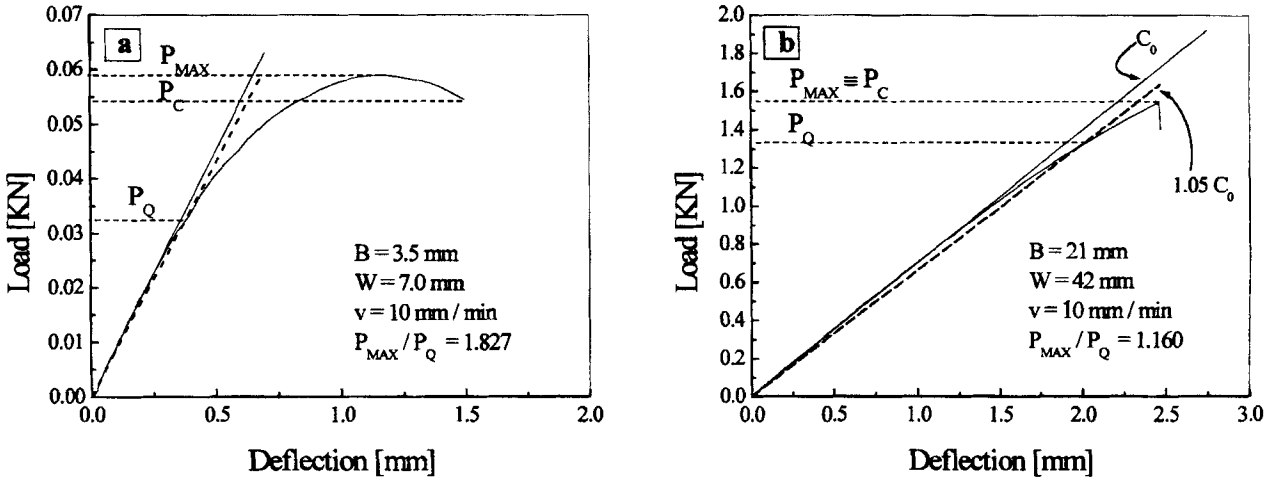

Fig. 2. Load-displacement diagrams: a) 3.5 mm thick specimens, b) 21 mm tick specimens (for the smallest specimens instability was reached beyond the maximum load).

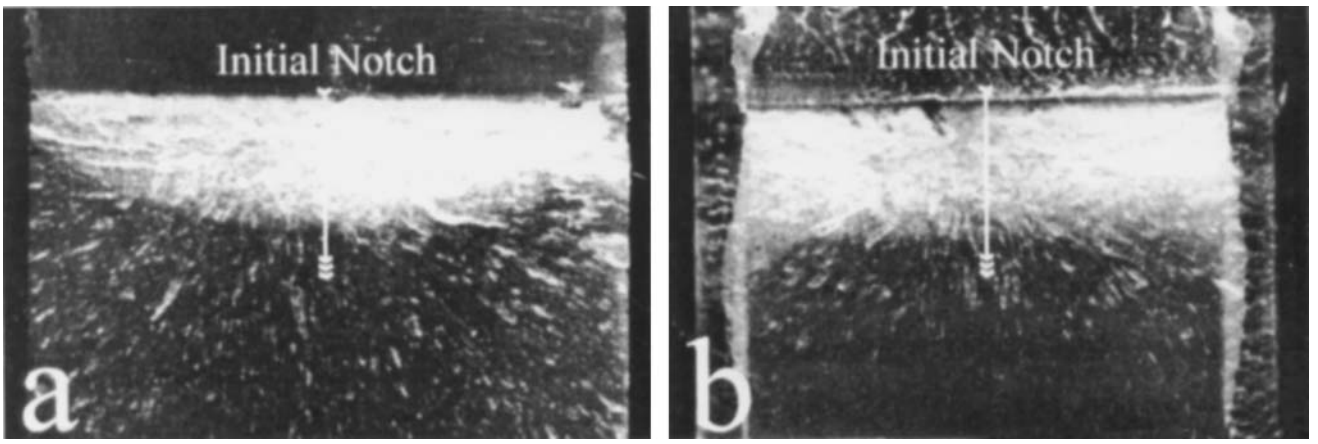

Fig. 3. Fracture surfaces. a: plane-sided specimen, b: sidegrooved specimen. Arrows indicate crack propagation direction.

tearing Δa that can be achieved was limited by the onset of cleavage instability.

The whitened plastic zone tapers inward as the distance from the crack front increases, which can be discerned in *Fig. 3a*. This may be caused by a transition from a plane strain state in the center of a specimen to a plane stress state in the surface regions, as previously denoted (1). Fernando and Williams (1) assumed that in polypropylene, the additional toughness stems from a plane stress skin effect, although they were not able to separate the exact contributions from crazing and shear yielding. The fact that in the center of the smooth specimen the crack and the whitened halo had propagated further ahead than at the edges of the crack front indicates that the more critical three-dimensional stress state generated in the interior of the material governs damage evolution (mainly crazing) (1) as well. The through-thickness differences in constraint may be avoided by sidegrooving (*Fig.3b*), which promotes triaxiality even at the edges of the sample, as can be appreciated from the more straight shape of subcritical growing and damaged zone.

The shattering effect mentioned above was described previously (2, 20). Fernando and Williams (2) noted that a single crack path was not observed within the whitened region, but that crack bifurcated and propagated in many directions when proceeding through the rest of the specimen. This phenomenon is clear evidence of excessive strain energy being dissipated during unstable fracture, suggesting that the crack propagates from a region of high local toughness at the crack tip to one of low toughness in the rest of the specimen. *Figure 4* shows evidence of crack path deflection. It can be appreciated that fracture did not occur at the midplane of the process zone but at the interface between the crazed zone and the bulk material. By comparing both fractographs it can be distinguished that the stress-whitened material remained in only one of the two halves (*Fig. 4a*). The fracture nucleus where the instability had generated is also discernible in the photograph (17, 21).

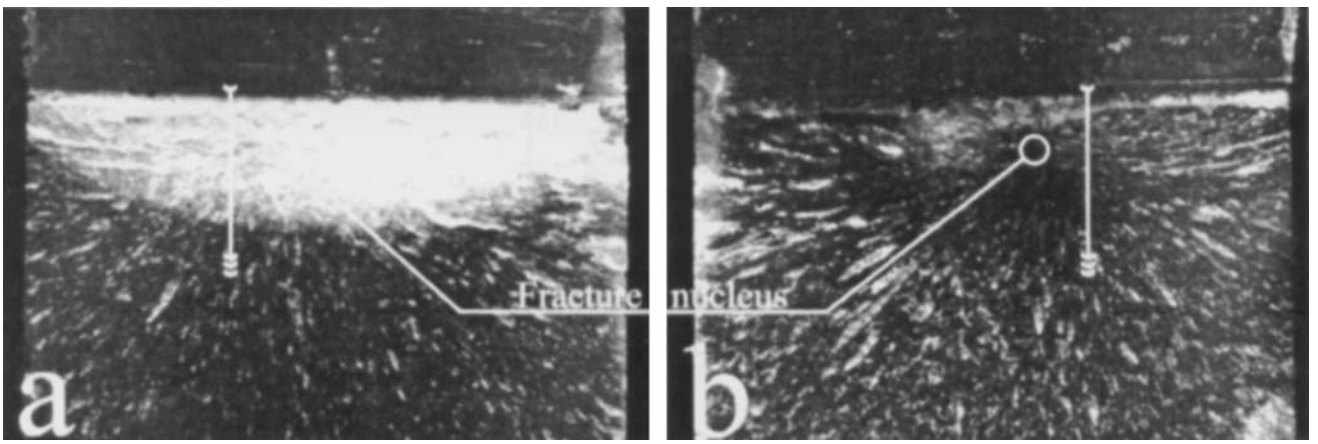

Fig. 4. Fracture surfaces of the two halves of the same sample showing: a: damage zone, b: Instability initiation point. Arrows indicate crack propagation direction.

Specimen Size Effects

An attempt to understand the nature of phenomenology was made by taking into account geometric constraint effects (thickness, sidegrooving, and ligament length), which affect the stress triaxiality and the size of plastic zone at the crack tip. The constraint requirements mentioned in the fracture mechanics parameters section (*Eq 5*) aim to ensure that the critical specimen dimensions, B, a, and (W-a), are at least ~50 times larger the radius of the plain strain plastic zone size (22, 23). Sidegrooving has the effect of removing plane stress zone at the edges (22, 24, 25).

The third constraint requirement (*Eq 6*) (26) accounts for the following situation: a fracture toughness test that displays considerable plastic deformation prior to failure. If the specimen fails well beyond P_Q, owing a large degree of nonlinearity, the K_Q value in this case would grossly underestimate the true toughness of the material. Consequently, the third validity requirement is necessary to ensure that a K_{IC} value is indicative of the true toughness of the material.

Figure 2 shows two load-displacements plots obtained at the two extreme specimen thicknesses assayed. Plots were always nonlinear, and with the exception of only very thin samples (*Fig. 2a*), instability was reached before maximum load (*Fig. 2b*). A slight tendency to gain linearity was detected with the increase in specimen thickness. However, valid test conditions are impossible to reach under practical situations (*Fig. 5*) because of the difficulties in molding specimens thicker than 20 mm. The fracture mode has never completely changed into complete cleavage, and ductile tearing (*Fig. 3*), even if inhibited to acceptable values (21, 22), was not completely suppressed.

In the specimen size range examined, values of K_{MAX} measured with geometrically similar specimens were not observed to decrease consistently with increasing thickness (*Fig. 6*) approaching an asymptotic minimum value as expected (27–29). Kaufman and Nelson reported a similar tendency for an aluminum alloy (23). Scatter bands of each specimen thickness overlapped and to test specimens large enough for fracture to occur under dominant linear-elastic conditions is not practically possible.

Figures 5 and *7* clearly show that linearity in load-line-displacement plots and valid K_{IC} test values are rarely possible under reasonable geometric experimental conditions since K_Q follows the same monotonically raising trend with thickness of K_{lim}, which stem from requirements criteria.

In the case of sidegrooved specimens, a straighter damage zone profile is observed due to the additional constraint generated at the edges (*Fig 3b*). However, moderate sidegrooving of the specimen does not appear to have a significant effect on the linearity of load-displacement plots (*Fig. 5*), probably because no necking was observed in the edges. The use of non-proportional specimens, which can alter in-plane constraint (21) (B/W ≈ 0.37 and 0.23 in (*Fig. 5*) was ineffective as well in promoting load-line displacement plot linearity. This behavior might be due to the difference in

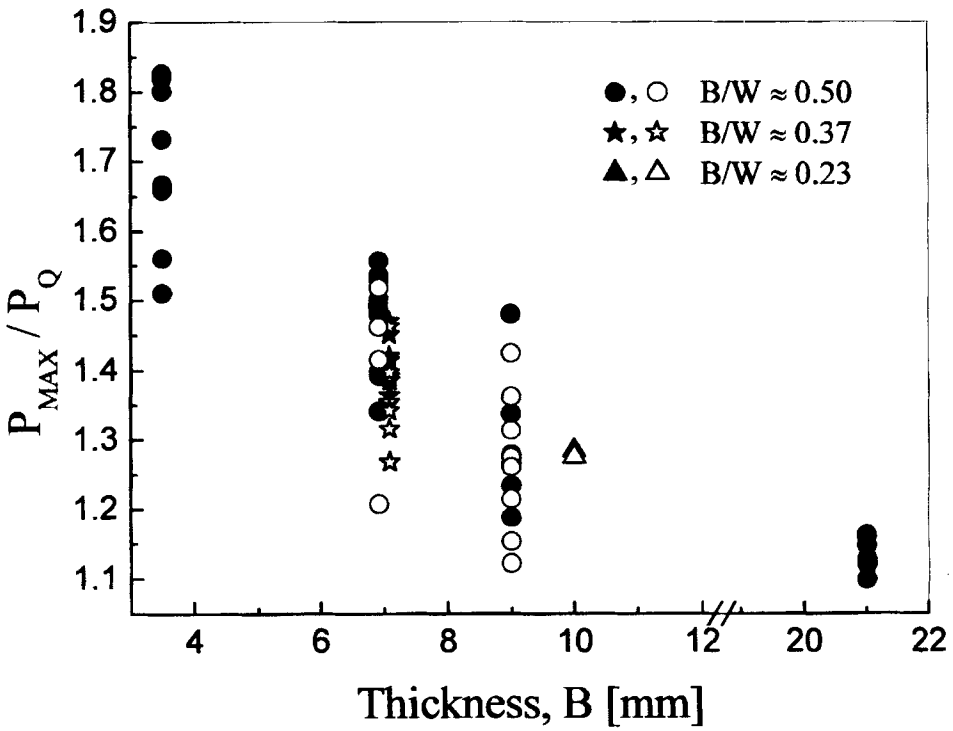

Fig. 5. Size effect on the linearity parameter (P_{MAX}/P_Q). Open symbols: side-grooved specimens.

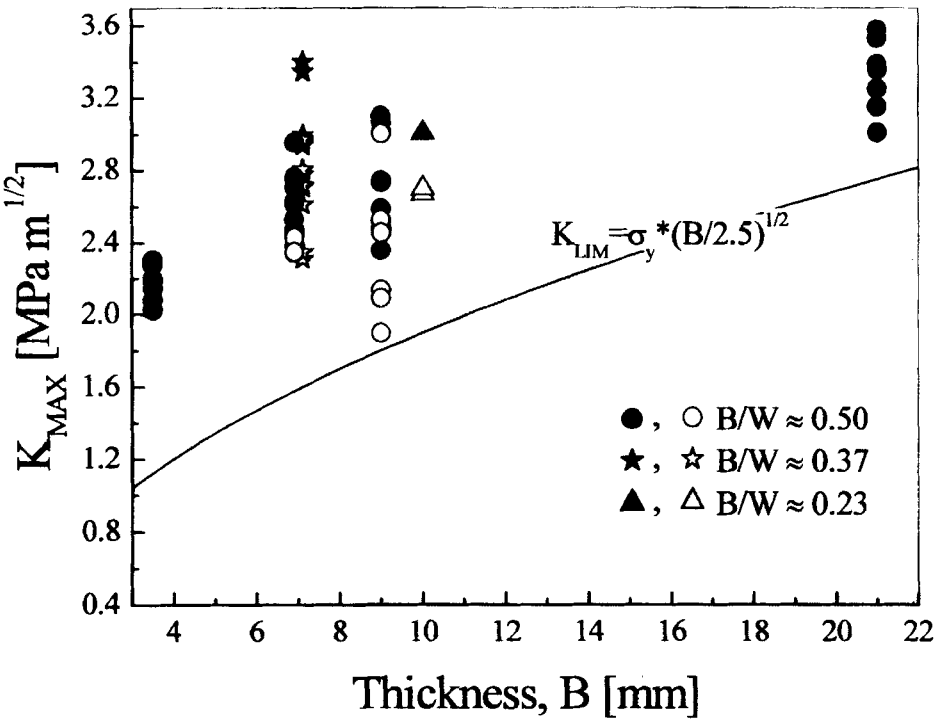

Fig. 6. Size effect on the linear elastic fracture parameter, K_{MAX}. Open symbols: sidegrooved specimens.

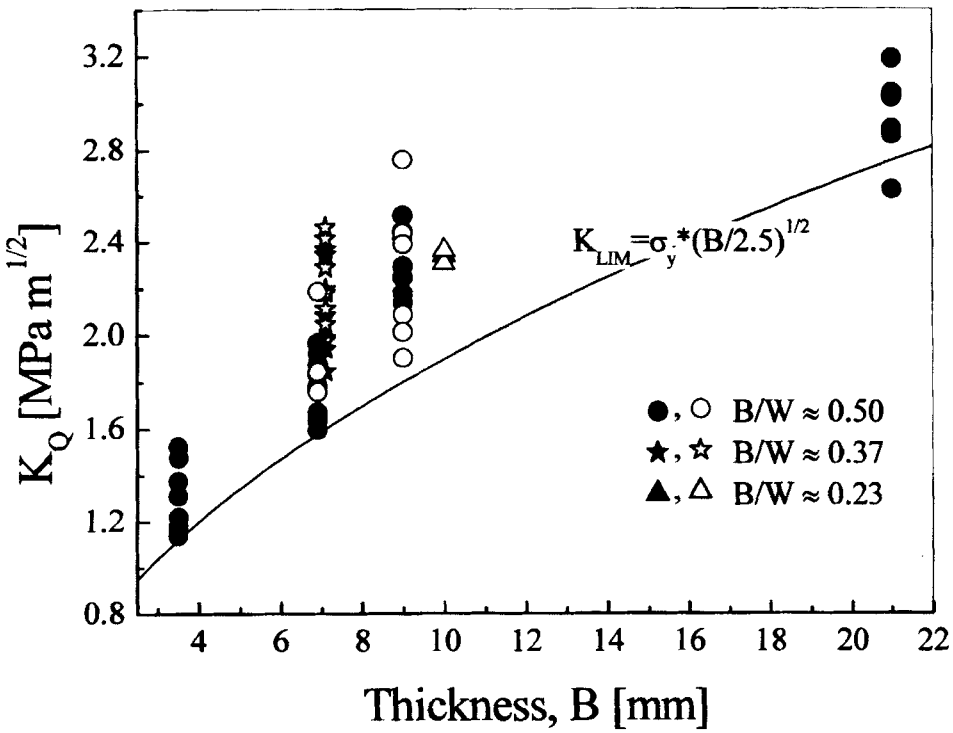

Fig. 7. Size effect on the linear elastic fracture parameter, K_Q. (K_{lim} sets the maximum K_Q valid value according to ASTM standards requirements).

nature of damage mechanism between PP and metals (30), since crazing is a dilatational mechanism, and then it is still active under high triaxial conditions.

In consequence, the currently accepted procedures (4–6) for measuring the plane-strain fracture toughness in polymers, K_{IC}, are strictly not applicable. On the other hand, the extrapolation to infinite thickness, a common practice in the literature (2, 31) at testing temperatures below room temperature, appears somewhat meaningless because of the large scatter. Thus, novel approaches should be used to determine critical parameters.

Scatter in Measurements and the "Weakest Link" Model

One of the most characteristic features of our results is that data is highly scattered in terms of J_C, as shown in *Fig. 8*. The most developed approach for explaining scatter and size effects of fracture toughness has been deduced from the weakest link theory and applied to data in steels in the ductile-brittle transition region (17, 18, 21, 32, 33). This theory assumes that small regions of very low toughness, called weakest links, are randomly distributed in the material. Failure occurs if at one of these weakest links the critical stress is reached. The load of fracture depends on the location of the "weak link" in the volume ahead of crack tip and on the critical stress of the individual weak link. Some plastic deformation and even stable crack growth may occur at the crack tip before cleavage takes place (17, 18, 21, 32). Under weakest link controlled cleavage the fracture shows one single dominant initiation site (21). The existence or nonexistence of these sites could provide a powerful means of indicating when link mode is operating.

The schematic model seems in principle to be consistent with all the macroscopic observations, which have been made concerning PP homopolymer fracture phenomena. Moreover, Varga (34) and Greco and Ragosta (35) also showed that spherulite boundaries constitute the "weak sites" of the polypropylene, and failure of the material is often initiated on these spots by coalescence of micro voids, cracks, and crazes. The "weak site" feature of spherulite boundaries is also derived from the fact that the majority of the noncrystallizing component is accumulated in these regions. Varga explained that spherulite boundaries act at weak sites, and failure often initiated at these spots. The fracture process is essentially controlled by the interconnections within the material (which in turn determine the craze structure).

In order to quantify the scatter of toughness, the thickness effect, and the effect of stable crack extension observed in some ferritic steels, a variety of statistical models have been developed (17, 18, 21). These models assume that the scatter band of the fracture toughness values can be modeled using Weibull statistics.

We chose the three-parameter Weibull cumulative frequency distribution to fit J_C distributions (32):

$$P_f = 1 - esp\left\{-\left[\frac{(J - J_{min})}{(\Theta - J_{min})}\right]^b\right\} \qquad (10)$$

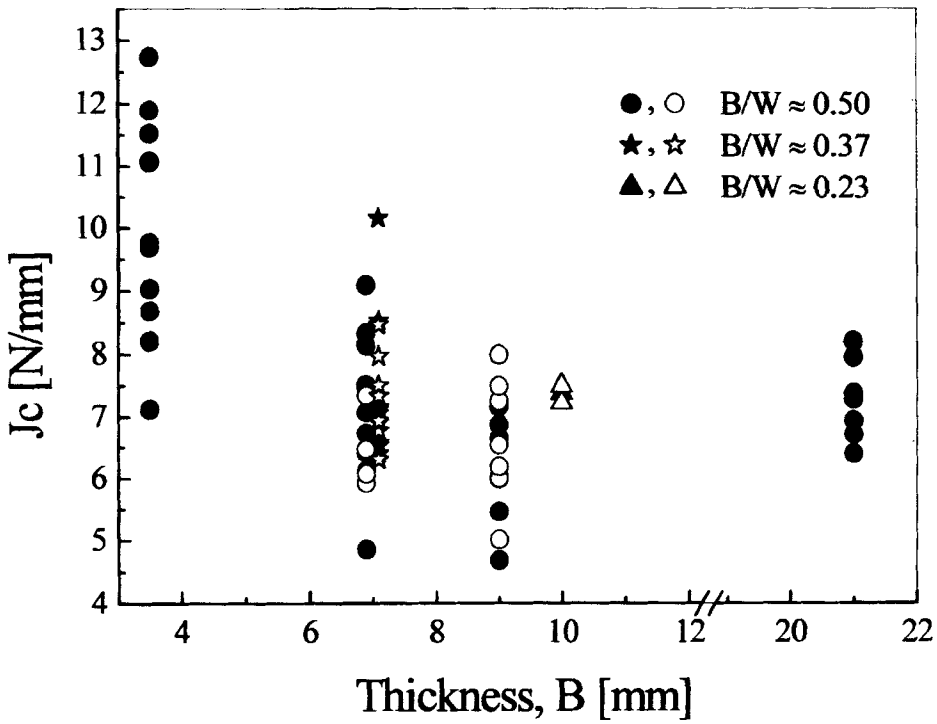

Fig. 8. Size effect on the critical elastic-plastic fracture parameter, J_C.

The three fitting constants are Θ, b, and J_{min}, which are the scale parameter ($J_C = \Theta$, when $P_f = 0.632$), the Weibull slope, and the lower-bound toughness value that defines a lower limiting toughness for specimens of infinite thickness, respectively.

Fitting parameters were determined by linear least square fitting of the double logarithm version of *Eq 10*. All three Weibull constants were adjusted to get an optimum linear fit to the data (32, 33). Results are shown in *Table 1*. A good data correlation was found only for specimens having a nominal thickness of 21 mm and displaying a fitted Weibull slope very close to 2 (*Fig. 9*). Several authors have proposed that this value is consistent with the structural steel micromechanics theory (see, for, instance, refs. 18, 33, 36).

The application of Weibull statistics on thinner specimens was unsuccessful. Some parameters showed physical inconsistency (*Table 1*) while the scale parameter inferred from thinner specimens distributions ($\Theta_1 = \Theta_2 (B_2/B_1)^{1/b}$) did not agree with the one determined in 21 mm samples as the weakest link model predicts (21). It has been shown theoretically (21) that so long as no stable crack extension occurs during the loading, and the constraint in the specimen does not change, which means that the triaxiality of the stress and strain field at the crack tip does not change during the loading event, the scatter band follows the Weibull distribution. The initiation of stable crack growth also affects the stress and strain fields ahead of the tip and may also influence the probability of triggering cleavage. McCabe *et al.* (32) stated that slow crack growth before the onset of cleavage cracking is, for various hypothetical reasons, reputed to cause a disruption of the local crack-tip stress field. Ostensibly, the propensity for the onset of cleavage fracture is changed from that of a specimen with a nongrowing crack. So, the large stable crack growth levels displayed by specimens thinner than 21 mm invalidated the application of Weibull approach. Despite some attempts trying to make crack growth adjustment are available in literature, the real value of these corrections is still controversial and they lack in the definition of full constraint fracture parameters (32).

Table 1. Weibull Fitting Parameters.

B*W	N	Best fit of Data		
		Slope	Θ [N/mm]	J_{min} [N/mm]
3.5* 7	10	2.739	10.56	5.40
7 *14	11	5.185	7.54	1.60
9 *18	7	7.342	6.70	<0.0
9 *18[a]	8	3.675	6.92	3.32
21*42	7	1.979	7.44	6.00

[a]Sidegrooved specimens.

J-R Curves Analysis and Prediction of a Permissible Extent of Ductile Crack Growth

When stable crack growth is present, in principle, fracture can be characterized by using the J-R analysis.

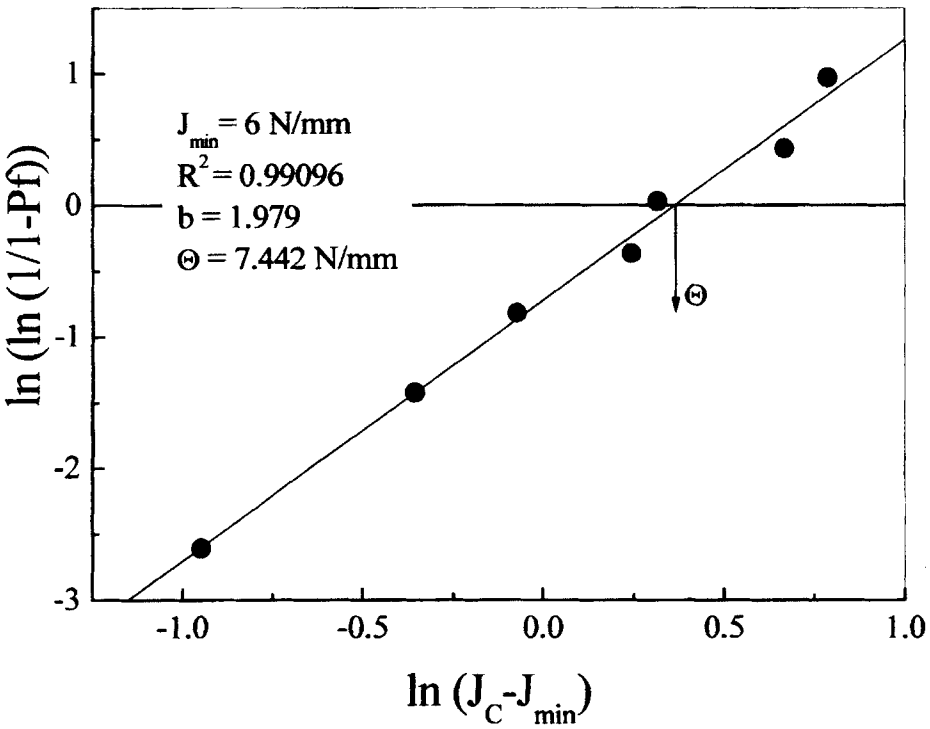

Fig. 9. Weibull plot.

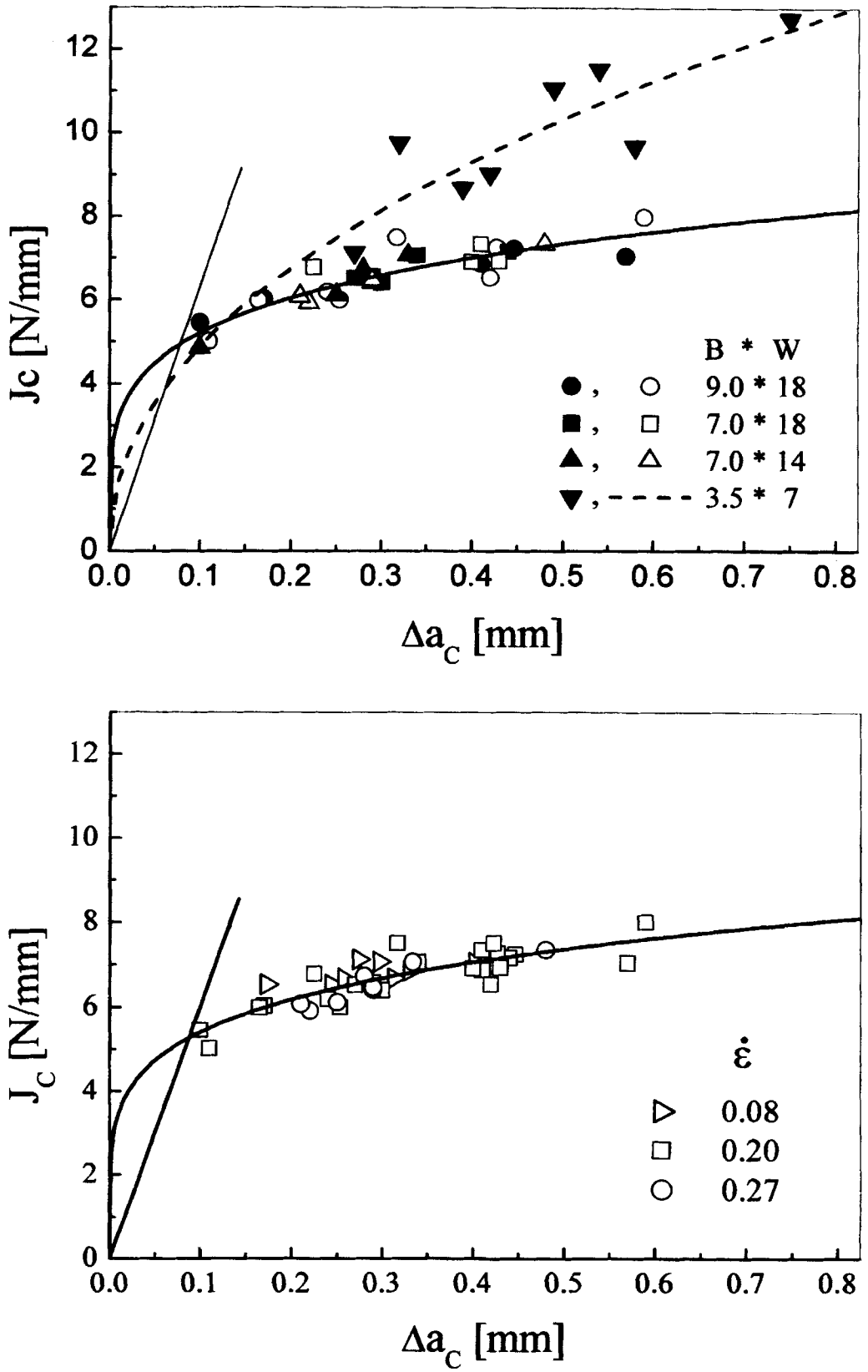

Fig. 10 Multispecimen J-R curve based on ductile crack growth value at instability a: specimens assayed at 10 mm/min. b: Strain rate effects on multispecimen J-R curve.

As known, existing restrictions regarding the ligament size are different for the linear-elastic parameter, K_{IC}, and the elastic-plastic parameter, J_{IC}. When applying K_{IC}, a much larger ligament is needed to get a "valid" result than that when applying J_{IC}. The more stringent ligament requirements with K_{IC} come mainly from the need to ensure that the specimen behaves in a nearly linear-elastic manner (Small Scale Yielding).

Figure 10 show graphics of J_C vs. subcritical growth (Δa) obtained under different geometry and loading conditions. Some specimens, even if theoretically identical, failed with little stable crack growth while other specimens sustained high levels of ductile tearing prior to cleavage. For the specimens that exhibited low toughness, the distance between crack tip and instability initiation was small. That means that a critical nucleus was available near the crack tip (*Fig. 4*). In the specimen that exhibited high toughness, there were no critical particles near the crack tip; the crack had to grow and sample additional material before a critical nucleus was found (18, 37). Our results showed that the measured distance from the initiation site to the original crack tip correlated very well with the measured fracture toughness.

To sum up, the amount of pre-cleavage ductile tearing, Δa, was not constant and showed scatter similar to that for the fracture toughness. Its magnitude was limited by the onset of cleavage instability so that a predetermined amount of ductile tearing cannot be guaranteed (*Fig. 11*). On the contrary, Vu-Khanh and Fisa (20) found that the location of fracture initiation at a certain distance ahead of the crack tip has a characteristic critical value. Therefore, in agreement with the strain energy density theory, they postulated that the subcritical crack growth can be considered a material parameter for predicting fracture instability.

J-R curves, however, are found to be size independent for specimen thickness larger than 7 mm as shown in *Fig. 10a*. A significant size effect appears only for very thin specimens (3.5-mm-thick samples). This is the usual tendency for small specimens to produce higher values of fracture toughness than larger ones. These latter specimens fell under conditions well beyond those for J-validity ($B < 15\ J_C/\sigma_y$) (38). The effect can be explained in terms of the reduced constraint in the smaller specimens and in terms of the higher probability of a region of low toughness material occurring close to the crack tip in the larger specimens. J-resistance curve values, obtained from specimens with $B \geq 7$ mm meeting the condition $B \geq 30\ J_C/\sigma_y$, superimposed the same dispersion data band. In this regime, cracks growing initially by a ductile mechanism follow the J resistance curve until cleavage occurs.

In general, loading rate effects have been neglected in standards (4–6, 39, 40), although it is well known that polymer fracture behavior is time dependent (41), because of the viscoelasticity nature of polymer behavior. In order to consider rate effects, data having the same nominal initial rate (*Eq 1*) were plotted together. No significant changes in trends were found (*Fig. 10b*).

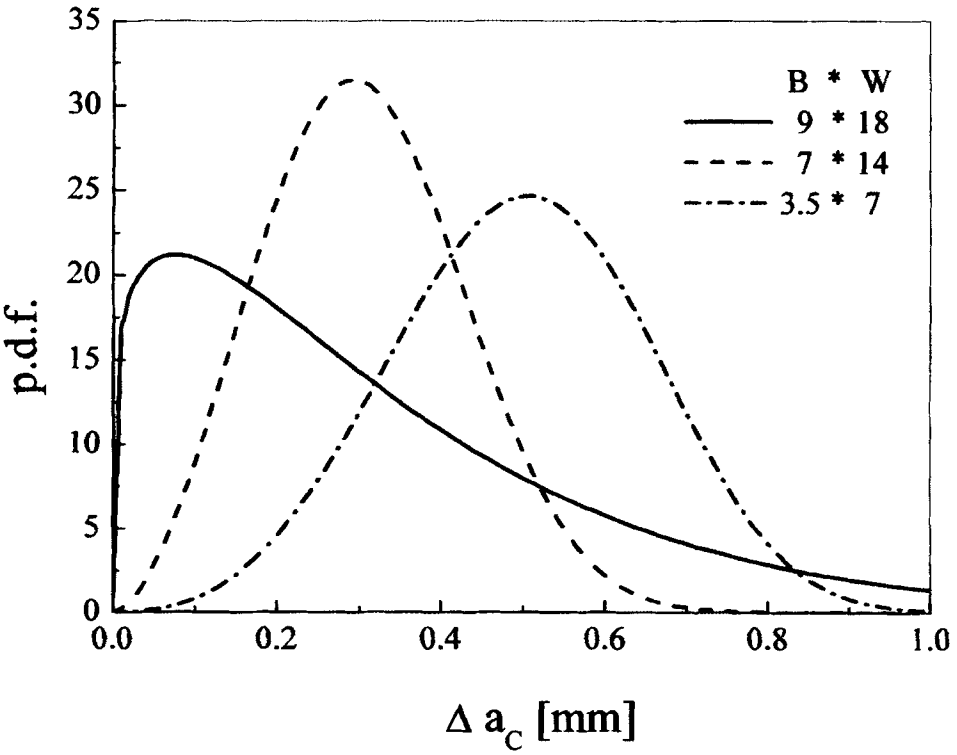

Fig. 11. Probability density functions as function of subcritical crack growth observed for various specimen sizes.

When the data point met the so-called "*J*-valid conditions", the *J*-resistance curves could be considered size independent within an acceptable scatter. However, neither the level of *J* at which the brittle fast fracture mechanism intervenes nor a critical value of Δa can be guaranteed. Thus, none of them can be taken as a characterizing parameter (*Fig. 10*). Milne and Curry (42) developed a phenomenological descriptive model, consistent in principle with our observations, that aims to estimate the amount of ductile crack growth permissible when ductile crack growth preceded the cleavage phenomenon. They defined K_{IC} as the fracture toughness at the onset of the brittle mode of fracture and K_{IJ} as the fracture toughness at the onset of ductile crack growth, then $K_{IC} > K_{IJ}$. Below K_{IJ} crack growth is due to blunting. The ductile crack extension obtained between the initiation of ductile crack growth and the onset of brittle is defined by the elastic-plastic crack growth resistance curve. K_{IC} cannot be reached without generating the appropriate amount of ductile crack extension.

Based on the latter considerations and taking into account that Weibull did not work in a reasonable range of specimen thickness, we suggest constructing a J-R curve from *J* and Δa values obtained at instability points. A J_{IC} can be taken from the intersection between the blunting line and J-R curve and then converted into K_{JIC} from *Eq.9*. This latter parameter sounds more reasonable as a design parameter since stable crack growth cannot be guaranteed and it is also a conservative criterion. The so-obtained J_{IC} values did not present physical crack growth. The derived K_{JIC} is the smallest one among the K_Q mean values obtained from the largest specimens and the threshold K_{Jmin} value from the Weibull approach (*Table 2*).

SUMMMARY AND CONCLUDING REMARKS

Different geometry dimensions that modify in-plane and out-of-plane constraints were used to assess the fracture behavior of PP homopolymer at varying testing rates and at room temperature. Under the testing conditions assayed, the so-called "valid K_{IC} values" could not be obtained since LEFM (4–6) requirements (as defined by *Eqs 5* and *6*) were not met.

Results appeared to be large scattered and size dependent. Large-scale yielding (judged from the damage zone developed at the crack tip and ductile crack growth) preceded brittle fracture and led to nonlinearity in load-line displacement curves. This behavior shows characteristics very similar to those shown by steels in the ductile-brittle transition regime (17–18–20–32).

The amount of pre-cleavage ductile tearing, Δa_c, showed differences among theoretically identical samples. However, the measured distance from the initiation site to the original crack tip correlated very well with the measured fracture toughness, which allows construction of J-R curves.

Our results showed that the level of subcritical crack growth that a sample can reach cannot be predicted from a J-R curve. Hence, it cannot be considered a material parameter for predicting fracture instability. The latter statement contradicts the findings of Vu-Khanh and Fisa (21).

It seems that the displayed behavior (ductile-brittle transition regime) is a direct result of the PP homopolymer micromechanism of fracture (34) that which initiates from microstructural defects present at the spherulite boundaries, which act as "weak sites" triggering brittle fracture. The location of this cleavage trigger relative to the crack tip dictates toughness. If this critical nucleus is near the crack tip, the toughness is relatively low; whereas a higher toughness can be measured if the cleavage trigger is relatively remote from the crack tip. In most cases, the crack will grow by ductile tearing until it reaches a microstructure feature that is capable of triggering cleavage.

In thick samples (21 mm) where negligible stable crack extension is present, the behavior seems to be in accordance with the weakest link model and the probability function can be obtained by fitting a Weibull distribution with a shape parameter of 2 through the toughness data point. On specimens thinner than 21 mm, apparent changes in constraint and stable crack extension influence the probability function, and therefore, no simple strategy for treating the size effects and scatter can be given for such a behavior.

In order to determine a lower bound toughness, as a compromise solution we proposed the subsequent protocol. To construct a J-R curve by plotting *J* values at the instability point, J_C, vs. the corresponding crack growth, Δa_c, and estimating K_{JIC} (*Eq 9*) from the intersection between the theoretical blunting line and J-R curve. Providing that each J_C point meets the condition $B \geq 30\ J_C/\sigma_y$, J-R curves are thickness independent despite the unavoidable scatter, and K_{JIC} represents the lower bound toughness (*Table 2*).

Table 2. Fracture Parameters From Different Methodologies

J – R Curves		Weibull	LEFM
K_{JIC} [MPa$\sqrt{m}$]		K_{JMIN}[MPa$\sqrt{m}$]	$\overline{K_Q}$ [MPa$\sqrt{m}$]
(Fig. 10a)	(Fig. 10b)	(Fig. 9)	(Fig. 7)
2.78	2.87	3.06	2.93

REFERENCES

1. P. L. Fernando and J. G. Williams,. *Polym. Eng. Sci.*, **21**, 1003 (1981).
2. P. L. Fernando and J. G. Williams. *Polym. Eng.* Sci., **20**, 215 (1980).
3. J. M. Hodgkinson, A. Savadori, and J. G. Williams, *J. Mater. Sci.*, **18**, 2319 (1983).
4. D 5045 Standadrd Test Method for Plane-Strain and Energy Release Rate of Plastic Materials, *Annual Book of ASTM Standards* (1999).

5. J. G. Willams and M. J. Cawood, *Polym. Test.*, **9**, 15 (1990).
6. EGF Task Group on Polymers, "A Linear Elastic Fracture Mechanics (LEFM) Standard for Determining K_C and G_C for Plastics", Testing Protocol, London (1990).
7. I. Narisawa and M. Takemori. *Polym. Eng. Sci.*, **26**, 466 (1986).
8. D. E. Spahr, K. Friedich, J. M. Shultz, and R. S. Bailey. *J. Mater. Sci.*, **225**, 4427 (1990).
9. L -H. Lee, J. F. Mandell, and F. J. McGarry, *Polym. Eng. Sci.*, **27**, 1128 (1987).
10. P. M. Frontini and A. Fave, *J Mater. Sci.*, **30**, 2446 (1995).
11. C. J. Chou, K. Vijayan, D. Kirby, A. Hiltner, and E. Baer, *J Mater. Sci.*, **23**, 2521 (1988).
12. C. J. Chou, K. Vijayan, D. Kirby, A. Hiltner, and E. Baer, J. *Mater. Sci.*, **23**, 2533 (1988).
13. B. Wunderlich. *Macromolecular Physics*, **3**, 63, Academic Press, New York (1980).
14. S. Hashemi and J. G. Williams, *J. Mater. Sci.*, **19**, 3746 (1984).
15. ESIS Procedure for Determining Fracture Behaviour of Materials. ESIS P2-92 1992.
16. J. D. G. Sumpter and C. E.Turner, *ASTM STP 601*, 3 (1976).
17. J. D. Landes and D. H. Shaffer, *ASTM STP 700*, 368 (1980).
18. K.Wallin, *ASTM STP 1171*, 264 (1993).
19. T. L. Anderson, *Fracture Mechanics. Fundamentals and Applications*, 376, CRC Press. Inc. Boca Raton, Fla. (1995).
20. T. Vu-Khanh and B. Fisa, *Theoretical and Appl. Fract. Mech.*, **13**, 11 19 (1990).
21. J. Heerens, U. Zerbst and K. -H. Schwalbe, *Fatigue Fract.Engng.Mater.Struct*, **16**, 1213 (1993).
22. W. F. Brown Jr. and J.E.Srawley, *ASTM STP 410* (1966).
23. J. G. Kaufman and F.G. Nelson, *ASTM STP 559*, 74 (1974).
24. H. G. deLorenzi and C.F. Shih, *Int. J. Fracture*, **21**,195 (1983).
25. B. A. Crouch, *Int. J. Fracture*, **52**, 275 (1991).
26. R. L. Lake, *ASTM STP 590*, 208 (1976).
27. Second Report of Special ASTM Committee *Materials Research and Standards*, **1**, 389 (1961).
28. J. F. Knott, *Fundamental of Fracture Mechanics*, Butterworths, London (1973).
29. A. G. Atkins and Y.-W. Mai *Elastic and Plastic Fracture: Metals, Polymers, Ceramics, Composites, Biological Materials*, Ellis Horwood, West Sussex U. K. (1988).
30. R. J. Young and P. A. Lovell, *Introduction to Polymers*, 367, Chapman & Hall, London (1991).
31. Y. W. Mai and J. G. Williams, *J. Mater. Sci.*, **12**, 1376 (1977).
32. D. E. McCabe, J. G. Merkle and R. K. Nanstad, *ASTM STP 1207*, 215 (1994).
33. D. E. McCabe, *ASTM STP 1189*, 80 (1993).
34. J. Varga, *J. Mater. Sci.*, **27**, 2557, (1992).
35. R. Greco and G. Ragosta, *J. Mater. Sci.* **23**, 4171 (1988).
36. T. L. Anderson, D. Stientra, and R. H. Dodds, Jr., *ASTM STP 1207*, 186 (1994).
37. K. Wallin, *Engng. Fracture Mech.*, **32**, 449 (1989).
38. E1820 Standadrd Test Method for Measurement of Fracture Toughness, *Annual Book of ASTM Standards* (1999).
39. ESIS Technical Committee 4, Polymers and Composites, "A Testing Protocol for Conducting J-Crack Growth Resistance Curve Tests on Plastics" (March 1992).
40. (ESIS) European Structural Integrity Society, "Test Protocol for Essential Work of Fracture," Version 5 (October 1997).
41. R. A. Schapery, *Int. J.- Fract.*, **11**, 141 (1975). ibid. 369; 549
42. I. Milne and D. A. Curry, *ASTM STP 803*, II-278 (1983).